Volume 9 | Number 19 | 21 May 2017 | Pages 6189–6608

Nanoscale

rsc.li/nanoscale

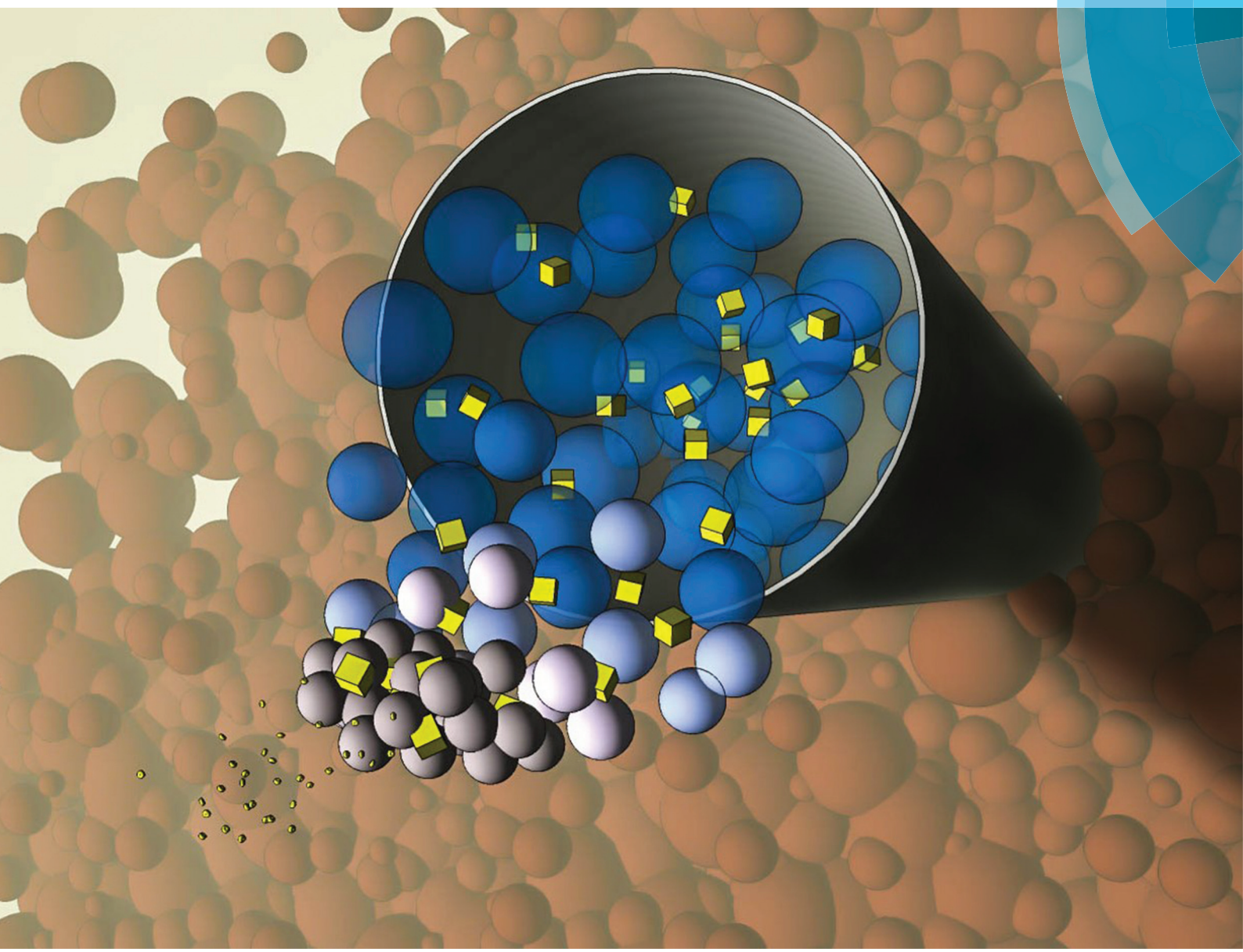

ISSN 2040-3372

ROYAL SOCIETY OF CHEMISTRY

PAPER

Tom O. McDonald *et al.*

Dual-stimuli responsive injectable microgel/solid drug nanoparticle nanocomposites for release of poorly soluble drugs

NCNST

Nanoscale

PAPER

View Article Online
View Journal | View Issue

Cite this: *Nanoscale*, 2017, **9**, 6302

Dual-stimuli responsive injectable microgel/solid drug nanoparticle nanocomposites for release of poorly soluble drugs†

Adam R. Town,[a] Marco Giardiello,[a] Rohan Gurjar,[b] Marco Siccardi,[b] Michael E. Briggs,[c] Riaz Akhtar[d] and Tom O. McDonald *[a]

An *in situ* forming implant (ISFI) for drug delivery combines the potential to improve therapeutic adherence for patients with simple administration by injection. Herein, we describe the preparation of an injectable nanocomposite ISFI composed of thermoresponsive poly(*N*-isopropylacrylamide) based microgels and solid drug nanoparticles. Monodisperse poly(*N*-isopropylacrylamide) or poly(*N*-isopropylacrylamide-*co*-allylamine) microgels were prepared by precipitation polymerisation with mean diameters of approximately 550 nm at 25 °C. Concentrated dispersions of these microgels displayed dual-stimuli responsive behaviour, forming shape persistent bulk aggregates in the presence of both salt (at physiological ionic strength) and at body temperature (above the lower critical solution temperature of the polymer). These dual-stimuli responsive microgels could be injected into an agarose gel tissue mimic leading to rapid aggregation of the particles to form a drug depot. Additionally, the microgel particles aggregated in the presence of other payload nanoparticles (such as dye-containing polystyrene nanoparticles or lopinavir solid drug nanoparticles) to form nanocomposites with high entrapment efficiency of the payload. The resulting microgel and solid drug nanoparticle nanocomposites displayed sustained drug release for at least 120 days, with the rate of release tuned by blending microgels of poly(*N*-isopropylacrylamide) with poly(*N*-isopropylacrylamide-*co*-allylamine) microgels. Cytotoxicity studies revealed that the microgels were not toxic to MDCK-II cells even at high concentrations. Collectively, these results demonstrate a novel, easily injectable, nanocomposite ISFI that provides long-term sustained release for poorly water-soluble drugs without a burst release.

Received 6th October 2016,
Accepted 18th March 2017

DOI: 10.1039/c6nr07858c

rsc.li/nanoscale

1. Introduction

Medication adherence to long-term therapy is vital in the successful treatment of chronic illness. However, data from the World Health Organization revealed that the average medication adherence lies at only 50% in developed countries and even less in the developing world.[1] Furthermore, potentially life threatening conditions can have a low adherence; for example, patients with diabetes display a mean adherence rate of only 67.5%.[2] One way to achieve higher adherence rates for chronic conditions is to simplify the drug regimen for the patient.[3] Daily oral doses can be replaced by a long acting system, which provides a sustained release of drug to maintain a blood plasma concentration at a therapeutic level. This has been shown to improve adherence by avoiding issues such as 'pill fatigue' and missed doses.[4,5] This is particularly the case for patients with psychological dysfunctions where oral medication compliance can be less than 40%,[6] or patients with drug addictions where large stocks of tablets cannot be provided.[7,8] Long acting systems can include injectable formulations,[9] polymeric implants,[10] microspheres,[11] mucosal inserts,[12] and topical patches.[13] These systems can be significantly more convenient for the patient and reduce healthcare costs by avoiding the effects of poor adherence such as hospital admissions. Initial implant systems were preformed and required micro surgery, or later the use of large hypodermic needles.[12] This led to the development of *in situ* forming implants (ISFI's).[14,15] These implants consist of an injectable drug formulation which solidifies after injection into the body,

[a]*Department of Chemistry, University of Liverpool, Crown Street, Liverpool, L69 7ZD, UK. E-mail: tomm@liv.ac.uk; Tel: +44 (0)151 795 0524*
[b]*Department of Molecular and Clinical Pharmacology, University of Liverpool, Block H, 70 Pembroke Place, Liverpool, L69 3GF, UK*
[c]*Centre for Materials Discovery, University of Liverpool, Crown Street, Liverpool, L69 7ZD, UK*
[d]*Department of Mechanical, Materials and Aerospace Engineering, School of Engineering University of Liverpool, George Holt Building, Brownlow Hill, Liverpool, L69 3GH, UK*
†Electronic supplementary information (ESI) available. See DOI: 10.1039/c6nr07858c

to form a depot, *i.e.* a site with a large storage of drug from which sustained drug release can occur over a long period of time. A number of ISFI systems have been developed, which achieve *in situ* gelation or solidification by different methods such as chemical or physiochemical cross-linking,[16,17] solidifying organogels,[18] and *in situ* phase separation.[19] ISFIs can suffer from many issues and limitations, and to our knowledge an ISFI without any has yet to be developed. These include a large burst release of drug,[20] potential toxicity of materials,[17] cytotoxicity and inflammation response,[10] long-term stability of the drugs,[16] mechanical stability of the depot,[21] limit to injection depth,[22] pre-heating before injection,[23] and variation in the shape of the implant formed, which leads to a variation in the amount of drug released.[24]

With over 60% of new drug candidates estimated to be poorly water soluble,[25] there is a need for an ISFI that could deliver poorly soluble drugs with enhanced control of release rate. One way to increase the solubility of poorly water soluble drugs is to formulate the drug into solid drug nanoparticles (SDNs).[26–30] These are nanoparticles formed solely of drug and stabilised by polymers and surfactants. SDNs have already been demonstrated to increase the bioavailability of drug when orally dosed.[31] SDNs have also previously been demonstrated as long acting injectable formulations,[32] requiring repeated monthly injections. We hypothesised that the release rate of drug can be tuned by entrapping SDNs in an ISFI, so that for potent drugs, the injection frequency can be lowered.

Poly(*N*-isopropylacrylamide) (PNIPAm) is a well-established thermoresponsive polymer that can be prepared in the form of nanoparticles known as microgels.[33–38] PNIPAm microgels swell in response to temperature,[39] exhibiting a volume phase transition temperature (VPTT), which is similar to the lower critical solution temperature (LCST) of linear PNIPAm.[40] Below the VPTT the polymer exists as hydrophilic particles, with the network swollen by water molecules. This is due to favourable hydrogen bonding between the amide units of the PNIPAm and water.[36] Above the VPTT, the polymer–polymer hydrogen bonding becomes more favourable and the particles de-swell as they expel solvent, resulting in a dramatic decrease in the diameter of the particle. PNIPAm microgels typically display both steric and electrostatic colloidal stability; below the VPTT the polymer chains extend out into solution and provide steric stabilisation,[39] while the charged chain end (derived from use of an initiator such as potassium persulfate (KPS)) gives the particles electrostatic stabilisation.[41] Above the VPTT, the electrostatic repulsion between particles provides colloidal stability, despite the collapse of the chain ends providing steric stabilisation.[42] However in the presence of salts, such as that of physiological fluid, flocculation occurs as the charges are screened.[43] Such behaviour allows dual-stimuli responsive microgels to be designed. The flocculation of the microgels has previously been used to both block membrane pores[44,45] and release drug.[46]

We hypothesised that by utilising the dual-stimuli responsive properties of PNIPAm microgels with SDNs we could produce a nanocomposite ISFI that forms a depot upon injection into a tissue environment. In the work presented here, SDNs are combined with a PNIPAm microgel in a liquid formulation which can then be injected into a depot site. Here, rapid aggregation of the microgel particles entraps the SDNs in a polymer network, forming a nanocomposite depot for sustained drug release. Premature aggregation in the injection needle is avoided as the microgels only aggregate in the presence of both the elevated temperature and salt when they have left the injection needle (see Fig. 1). In this article, we demonstrate the following: the efficient entrapment of payload nanoparticles within a nanocomposite; that the rate of drug release from a nanocomposite containing SDNs can be controlled by blending microgels with different comonomer compositions and show that such ISFIs display sustained release profiles exceeding 120 days with very little burst release.

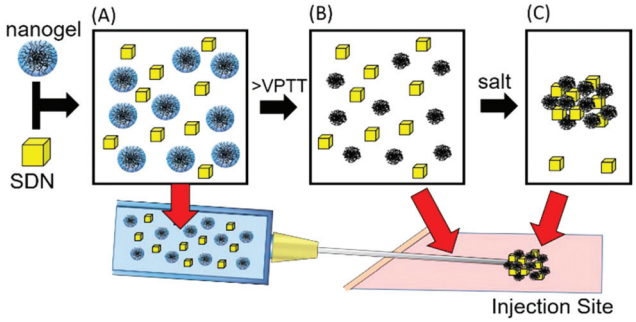

Fig. 1 Microgel/solid drug nanoparticle composite ISFI system (A) microgel/SDN solution loaded into syringe (B) de-swelling of microgel particles in hypodermic needle above VPTT (C) aggregation of microgel particles entrapping SDNs at depot site, due to contact with salt.

2. Experimental section

2.1 Materials

N-Isopropylacrylamide (NIPAm, Sigma-Aldrich), allylamine (AlA, Sigma-Aldrich), azobisisobutyronitrile (AIBN, Sigma-Aldrich) *N*,*N*-methylenebis(acrylamide) (BIS, Sigma-Aldrich), potassium persulfate (KPS, Sigma-Aldrich), oil red O (OR, Sigma-Aldrich), agarose (Sigma-Aldrich), sodium chloride (NaCl, Sigma-Aldrich), styrene (Sigma-Aldrich), phosphate buffered saline tablets (PBS, Fischer Scientific), 50% (w/v) aqueous poly(acrylic acid) (P(AcA), $\bar{M}_n$ = 2000, Sigma-Aldrich), tetrahydrofuran (THF, Fischer Scientific), ethanol (EtOH, Fisher Scientific), HPLC grade acetonitrile (MeCN, Fisher Scientific), dichloromethane (DCM, Sigma-Aldrich), polyvinyl alcohol (PVA grade 4–88, MW 57–77 000, Sigma-Aldrich), Kolliphor TPGS (BASF), potassium phosphate monobasic (KH_2PO_4, Sigma-Aldrich), orthophosphoric acid solution 50% (KH_2PO_4, Sigma-Aldrich), hydrochloric acid 37% (HCl, Fischer Scientific), anhydrous sodium hydroxide pellets (NaOH, Sigma-Aldrich), CellTiter-Glo® substrate (Promega), CellTiter-Glo® buffer (Promega), 3-(4,5-dimethylthiazol-2-yl)-2,5-diphenyltetrazolium bromide (MTT, Sigma-Aldrich), dulbecco's modified eagle's medium (DMEM, Sigma-Aldrich), rotenone (Sigma-Aldrich), Hank's balanced salt solution (HBSS, Sigma-

Aldrich), MDCK-II cell lines (Sigma-Aldrich), *N*,*N*-dimethylformamide (DMF, Sigma-Aldrich), sodium dodecyl sulfate (SDS, Sigma-Aldrich) were all used as received. The model drug used was lopinavir (LPV, WuXi PharmaTech). Type I distilled water obtained from a water purification system had a resistivity of >18 MΩ cm^{-1} (PURELAB option R, Veolia).

2.2 Synthesis of PNIPAm microgels

The PNIPAm microgels were synthesised by precipitation polymerisation. A summary of the formulation which was used for each microgel species can be found in Table 1. In a typical synthesis, the NIPAm monomer, AlA comonomer and BIS crosslinker were dissolved in distilled water (130 mL for PNA-00 and 160 mL for PNA-25) in a 250 ml two-neck round bottom flask equipped with a reflux condenser. This was then sealed and nitrogen was bubbled through the aqueous solution for 1 hour whilst stirring (400 rpm) to remove dissolved oxygen. The solution was then heated to 60 °C. Separately KPS initiator was dissolved in distilled water (3.75 mL for PNA-00 and 10.5 mL for PNA-25) and degassed with N_2 for 1 hour before being transferred to the flask containing the monomers. The reaction was maintained under a N_2 atmosphere for 4 hours at 60 °C before being cooled down to room temperature. To remove unreacted impurities, the microgel suspension was dialysed for 5 days using 12–14 kDa MWCO dialysis tubing, replacing the distilled water every 12 hours. The purified suspension was then lyophilised (Virtis Benchtop K with ultra-low temperature condenser) and sealed for storage.

2.3 Characterisation of PNIPAm microgels and aggregate material

Characterisation of the microgel dispersions and aggregates was carried out using dynamic light scattering (DLS), laser Doppler electrophoresis (LDE), scanning electron microscopy (SEM), ^{1}H nuclear magnetic resonance (NMR), potentiometric titration, Atomic force microscopy (AFM) and Fourier transform infrared spectroscopy (FTIR). DLS and LDE was performed using a Malvern Zetasizer Nano ZS (running Malvern Zetasizer software V7.11) (Malvern Instruments, Malvern, UK) with 633 nm He–Ne laser and the detector positioned at 173°. Dialysed samples were diluted to 1 mg mL^{-1}. The *Z*-average diameter was recorded in the range (20–50 °C) using a thermal equilibration time of 600 seconds in 1 cm path length disposable cuvettes. Measurements were repeated in triplicate to give a mean *Z*-average diameter and polydispersity index (PdI). Zeta potential measurements were performed using DTS1070 folded capillary cells (Malvern, UK). The pH of the sample was measured before performing zeta potential measurements, and for both samples fell in the range pH 7 ± 0.5. Capillary cells were flushed with ethanol and water prior to usage. The zeta potential measurement was made with a minimum of 10 and maximum of 40 runs, and the voltage applied was automatically selected by the software. To prepare the microgel dispersions for SEM imaging, the samples were diluted to 0.01 mg mL^{-1} in distilled water. 50 μL of solution was pipetted onto a circular cover glass (10 mm diameter) attached to a carbon adhesive disc on an aluminium SEM specimen stub (12.5 mm diameter). For SEM images of the aggregated material, swollen gel was formed in PBS and then adhered to a coverslip on an SEM stub. This was heated to 37 °C to induce aggregation. The samples were left to air-dry for 24 hours, followed by sputter coating with gold (EMITECH K550X) with a deposition current of 25 mA for 100 seconds before imaging. SEM images of the microgel morphology were then obtained using a Hitachi S-4800 FE-SEM at 3 kV. To record ^{1}H NMR spectra lyophilised microgel sample was dissolved in D_2O at 20 mg mL^{-1} and analysed on a Bruker 400 MHz spectrometer (Bruker, MA, USA). The potentiometric titration of PNA-25 was conducted with a 50 mL aqueous dispersion of PNA-25 at 1 mg mL^{-1}. The sample pH was then lowered below pH 4 using 0.1 M HCl. The sample was then titrated with 0.1 M NaOH at 25 °C ± 0.5 °C under a nitrogen atmosphere. A Hanna Instruments HI-11310 pH electrode (Hanna Instruments, Bedfordshire, UK) was used to record the change in pH. To record FTIR spectra a blank background scan was performed, followed by a recording of the spectra of lyophilised microgel *ca.* 5 mg, which was clamped onto the ATR crystal of a Bruker alpha platinum ATR (Bruker, Santa Barbara, CA, USA). Atomic force microscopy (AFM) was carried out using a Bruker Multimode 8 system (Bruker, Santa Barbara, CA, USA) operated with ScanAsyst Mode in ambient conditions. All testing was conducted using a Bruker RTESPA-150 probe with a nominal radius of 8 nm and a spring constant of 5 N m^{-1}. Each scan was conducted with a resolution of 256 pixels per line and with a scan rate of 0.799 Hz. The samples were prepared by placing a thin layer of swollen gel formed in PBS onto glass coverslips, which were then incubated at 37 °C in a water saturated atmosphere for 72 hours. The coverslips were then adhered to 15 mm diameter metal stubs for mounting in the AFM. The AFM images were analysed off-line using Bruker Nanoscope Analysis 1.7 software.

Table 1 The composition used in microgel synthesis

Sample	NIPAm (mol%)	AlA (mol%)	BIS (mol%)	KPS[a] (mol%)	[NIPAm] (mg mL^{-1})
PNA-00	94.3	—	3.6	2.1	5.8
PNA-25	70.9	24.8	2.7	1.6	25.0

[a] KPS dissolved at 20 mg mL^{-1} in distilled water.

2.4 PNIPAm microgel gelation and aggregation studies

The concentration at which the microgel samples formed a self-supporting gel was found by first adding 10 mg of material to 1 mL of phosphate buffered saline (PBS) in a glass vial with an internal diameter of 20 mm. Using the tube inversion method, the mass of microgel was increased in increments until the microgel no longer flowed upon inversion of the vial for 30 seconds. The % (w/w) of water contained in the microgel at 25 °C is calculated from the mass of freeze dried microgel and water in the swollen microgel formed from the tube inver-

sion method. After heating to 37 °C the aggregate was separated from the eluted solvent to determine its mass. The mass of microgel remains constant, so the difference in mass is due to any solvent remaining in the aggregate, allowing the % (w/w) of water at 37 °C to be calculated.

2.5 Tissue injection simulation

Agarose powder (0.5% (w/w)) was slowly added to a beaker of PBS whilst stirring, and then weighed, before covering the beaker with plastic wrap with a hole for ventilation, and heating to 95 °C for 10 minutes. Hot water was then added to bring the contents to the original weight. This was then cooled to 55 °C and cast into pre-warmed vials with an internal diameter of 20 mm. These were then left for 12 hours at 37 °C before use. PNA-25 at 6.2% and 2.0% (w/w) and PNA-00 at 14.9% and 5.7% (w/w) in distilled water were injected through a 18G hypodermic needle into 0.5% (w/w) agarose gel at 37 °C.

2.5.1 Polystyrene nanoparticle synthesis and oil red dye (OR) encapsulation. Polystyrene (PS) nanoparticles were prepared using modifications of a dispersion polymerisation method in which colloidal stability was provided by p(AcA).[47] Briefly, styrene monomer (15.35 mL) was dissolved in ethanol (26.23 mL) and distilled water (101.05 mL) in a 250 mL two-neck round bottom flask equipped with a reflux condenser. 50% (w/v) aqueous p(AcA) (2.92 mL) was then added along with KPS (234 mg) in distilled water (3.32 mL). This was then sealed and nitrogen was bubbled through the aqueous solution for 1 hour whilst stirring (400 rpm), to remove dissolved oxygen. The solution was then heated to 70 °C. The reaction was maintained under a N_2 atmosphere for 24 hours before being cooled to room temperature. The PS nanoparticle suspension was purified by centrifugation (Thermo Scientific Heraeus Megafuge 8R centrifuge) at a relative centrifugal force (RCF) of 10 900 in 50 mL centrifuge tubes for 1 hour, and washed with distilled water (*ca.* 50 mL), this process was repeated twice. OR was encapsulated into the particles by modifying a previous swelling-diffusion technique.[48] Firstly, the aqueous PS suspension (32 mg mL^{-1}, 25 mL) and aqueous Pluronic F127 (72 mg mL^{-1}, 8.3 mL) were added to a 50 ml centrifuge tube. This was vortexed at 3000 rpm for 60 seconds and then left for 24 hours on a tube roller (33 rpm). Tetrahydrofuran (THF) (16.66 mL, 33% (v/v)) containing oil red O (OR) (14.7 mg) was added to the suspension, and then vortexed at 3000 rpm for 600 seconds, followed by 0.5 hours on a tube roller (33 rpm). The colloid was then washed five times with distilled water using a centrifuge (RCF = 10 900, 1 hour) between washes and then lyophilised (Virtis Benchtop K with ultra-low temperature condenser). A sample of the PS nanoparticles with encapsulated OR was prepared at a concentration of 0.1 mg mL^{-1} and was analysed with DLS after synthesis and after lyophilisation.

2.5.2 Polystyrene nanoparticle entrapment study. In a glass vial with internal diameter 20 mm, 66.6 mg of PNA-25 was mixed with lyophilised PS nanoparticles of 10, 20 and 40% (w/w) relative to the microgel. After adding 1 mL of PBS the dispersion was left for 10 min to allow the lyophilised microgel to swell. The samples were then vortexed at 300 rpm to mix the PS nanoparticles through the swollen microgel dispersion. These samples were then heated (in a water bath) to 37 °C for 1 hour to form shrunken discs of aggregated microgel, with excess PBS expelled from the discs in the heating process. A negative control of microgel alone and positive control of PS particles alone were conducted alongside the samples. 0.2 mL of solution was removed for UV-visible spectrophotometric analysis (Thermo Scientific NanoDrop 2000c) with a 1 cm path length quartz cuvette at a wavelength of 565 nm (λ_{max} for OR). To determine the concentration of PS nanoparticles a stock solution of 1 mg mL^{-1} dispersed in PBS was serially diluted to form a linear calibration curve of absorbance at 565 nm against concentration in the range 1–100 μg mL^{-1}.

2.6 Lopinavir (LPV) solid drug nanoparticle (SDN) synthesis

The LPV SDNs were prepared by emulsion-spray-drying as described by Owen *et al.*[49] Briefly, a stock solution of LPV (200 mg mL^{-1} in dichloromethane (DCM)), polyvinyl alcohol (PVA grade 4–88, MW 57–77 000) (50 mg mL^{-1} in water), Kolliphor TPGS (50 mg mL^{-1} in water) were prepared. Three stock solutions were mixed in the LPV : PVA : Kolliphor TPGS ratio of 60 : 192 : 48 (mL) in a 1 : 4 DCM to water mixture. Emulsification was conducted using a Hielscher UP400S ultrasonic processor equipped with a H14 Probe at 100% output (140 W) for 180 seconds, with immediate spray-drying using a benchtop spray-dryer (BUCHI Mini-290) with an air-atomizing nozzle and compressed air as the drying gas. Spray-drying process conditions: 7 mL min^{-1} solution flow rate; 65 °C outlet temperature; 110 °C inlet temperature. Resultant powders were further dried under vacuum for 48 hours to remove residual DCM. SDN dispersions result from subsequent powder dispersion in water; for DLS characterisation, powders were dispersed in distilled water at 2 mg mL^{-1} (1 mg mL^{-1} *cf.* LPV).

2.7 Drug release in phosphate-buffer saline (PBS)

The *in vitro* drug release was performed using adaptations of the sample and separate method,[50] as performed in previous work.[51] The required amount of each lyophilised microgel, 6.24% (w/w) for PNA-25, and 14.90% (w/w) for PNA-00, was dispersed to form a swollen self-supporting gel in 1 mL of PBS (pH 7.4, 0.137 M NaCl and 0.0027 M KCl) in a glass vial of internal diameter 20 mm. To this 22.2 mg of LPV or 44.4 mg of LPV SDNs (50% (w/w) loading of LPV) were vortexed to give 22.2 mg of LPV per formulation. These were then heated to 37 °C for 1 hour to form shrunken discs with excess PBS expelled from the discs in the heating process, this was removed and used as the first release time point. These discs were transferred to larger 250 mL glass sample jars with 100 mL of fresh PBS. Subsequent release samples were taken at pre-determined intervals by removing 100 mL from the vessel and replacing with 100 mL of fresh PBS at 37 °C to prevent a saturation limit with a large excess of solvent. Release vessels were kept at 37 °C ± 0.5 °C in a water bath. The amount of LPV released was quantified by HPLC analysis.

2.8 HPLC procedure

The HPLC method is adapted from the method published by Giovanni Di Perri *et al.*[52] Briefly, HPLC grade acetonitrile (MeCN) (1.8 mL) was added to each release sample (4.2 mL) to create 30% (v/v) MeCN samples, followed by filtering through a 0.45 μm PTFE syringe filter. 40 μL of the solution was injected into a HPLC-PDA system (PerkinElmer Series 200). The mobile phase was composed of solvent A (KH_2PO_4 50 mM dissolved in HPLC grade water then pH adjusted with H_3PO_4 to reach pH 3.23) and solvent B (MeCN) with the gradient reported in Table 2. Chromatographic separation was performed with an Agilent ZORBAX Eclipse Plus 3.5 μm C18 column (100 × 4.6 mm ID, Santa Clara, CA) maintained at 25 °C in a column oven with a solvent flow rate of 0.5 mL min^{-1} giving a retention time of LPV of 9.6 ± 0.2 min. The PDA detector was set to 210 nm with a bandwidth of 2 nm. The concentration of LPV in the samples was calculated against known standards using the area under the chromatogram peaks. Three standards covering the concentration range of the HPLC method were used to verify the results, and samples were analysed in duplicate.

2.9 *In vitro* microgel cytotoxicity study

Cytotoxicity experiments were carried out on MDCK-II cell lines by MTT and ATP assay (Promega CellTiter-Glo® Luminescent Cell Viability Assay, Madison, WI). In both assays cells were seeded on 96-well plates at a density 2×10^4 cells per well in 100 μL of Dulbecco's Modified Eagle Medium (DMEM) and incubated for 24 hours. Ten different concentrations of the microgels were prepared by ten-fold serial dilution with the media, starting at 10 mg mL^{-1}. A ten-fold serial dilution of rotenone from 100 μM acted as a positive control, and cells alone in media as a negative control. Cells were incubated for 72 hours at 37 °C. In the ATP assay the wells were then equilibrated at room temperature for 30 minutes. 100 μL of Beetle Luciferin (CellTiter-Glo® Reagent) was added and mixed on an orbital shaker for 2 minutes to induce cell lysis. After incubation for 10 minutes at room temperature the luminescent signal was measured using a GENios microplate reader (TECAN). Samples were repeated in quadruplicate. The background luminescence of DMEM was subtracted from the sample luminescence. In the MTT assay after the 72 hour incubation period, 5 mg of MTT was dissolved in 1 mL of hank's balanced salt solution (HBSS). 20 μL was added to each well and incubated for 2 hours, followed by 100 μL of lysis buffer (50% DMF in water containing 20% SDS) for 12 hours. The absorbance of each well was measured at a wavelength of 560 nm using a GENios microplate reader (TECAN). Samples were repeated in quadruplicate. The absorbance of DMEM, and the absorbance of microgel interaction with MTT without cells present, was subtracted from the sample absorption.

Table 2 The solvent gradient used in the HPLC method

Time (min)	Solvent A % (v/v)	Solvent B % (v/v)	Flow (mL min^{-1})
0.0	70	30	0.5
1.0	70	30	0.5
3.0	30	70	0.5
11.5	30	70	0.5
12.0	70	30	0.5
12.5	70	30	0.5

3. Results and discussion

3.1 Preparation and characterisation of PNIPAm microgels

PNIPAm microgels were prepared *via* precipitation polymerisation before being characterised by dynamic light scattering (DLS), scanning electron microscopy (SEM), Fourier transform infrared spectroscopy (FTIR) and potentiometric titration. When the NIPAm monomer is used at a sufficiently low concentration (5.8 mg mL^{-1}) in aqueous solution, Table 1, narrow polydispersity microgel particles, PNA-00 (mean *Z*-average diameter = 567 nm, PdI = 0.24 at 25 °C) were produced, Fig. 2(A)(i). When the charged comonomer allyl amine (AlA) was introduced at 25 mol% the concentration of NIPAm in the synthesis could be increased, Table 1, whilst still obtaining monodisperse particles of a similar size, as in PNA-25 (mean *Z*-average diameter = 547 nm, PdI = 0.11 at 25 °C) Fig. 2(A)(ii). This was attributed to the comonomer providing electrostatic stabilisation of the particles during synthesis, preventing aggregation when the concentration of growing particles during synthesis is increased. SEM images show that discrete monodisperse particles were formed for both microgel samples PNA-00 and PNA-25, with a diameter corresponding to the *Z*-average diameter of the particles above the VPTT measured *via* DLS (approximately 250 nm). ^{1}H NMR and FTIR spectra is consistent with previous microgel characterisations, with all proton signals of PNIPAM accounted for (see ESI Fig. S1†) with a weak signal detected at 2.81 ppm for the CH_2 in the side group of the polyallylamine repeat unit.[53–55] NMR analysis also demonstrated that all unreacted monomers were removed during workup of the microgels as no vinyl peaks can be seen in the range 5.5–6.5 ppm. The FTIR spectra for the microgels were found to match that of previously studied PNIPAM microgels, however there was no noticeable difference between the IR spectra for PNA-00 and PNA-25. This was likely because the mol% of comonomer AlA incorporation was low or due to overlap between the signals for the primary amines of the poly (allyl amine) repeat unit compared to the signal from the amides from poly(*N*-isopropylacrylamide) (see ESI Fig. S2†).[36] Due to the lack of clear signals to prove allyl amine inclusion potentiometric titration was used to quantify the number of amines present in the sample.[38,56,57] This suggests 3.1 mol% AlA was incorporated into the microgel (see ESI Fig. S3†).

In order to investigate the dual-stimuli responsive properties of the microgel samples, the *Z*-average diameter and zeta potential of the microgels were measured at intervals over the temperature range 15 to 55 °C for both PNA-00 and PNA-25. As PNA-00 is heated in water the particles de-swell but remain colloidally stable, resulting in the dramatic decrease in

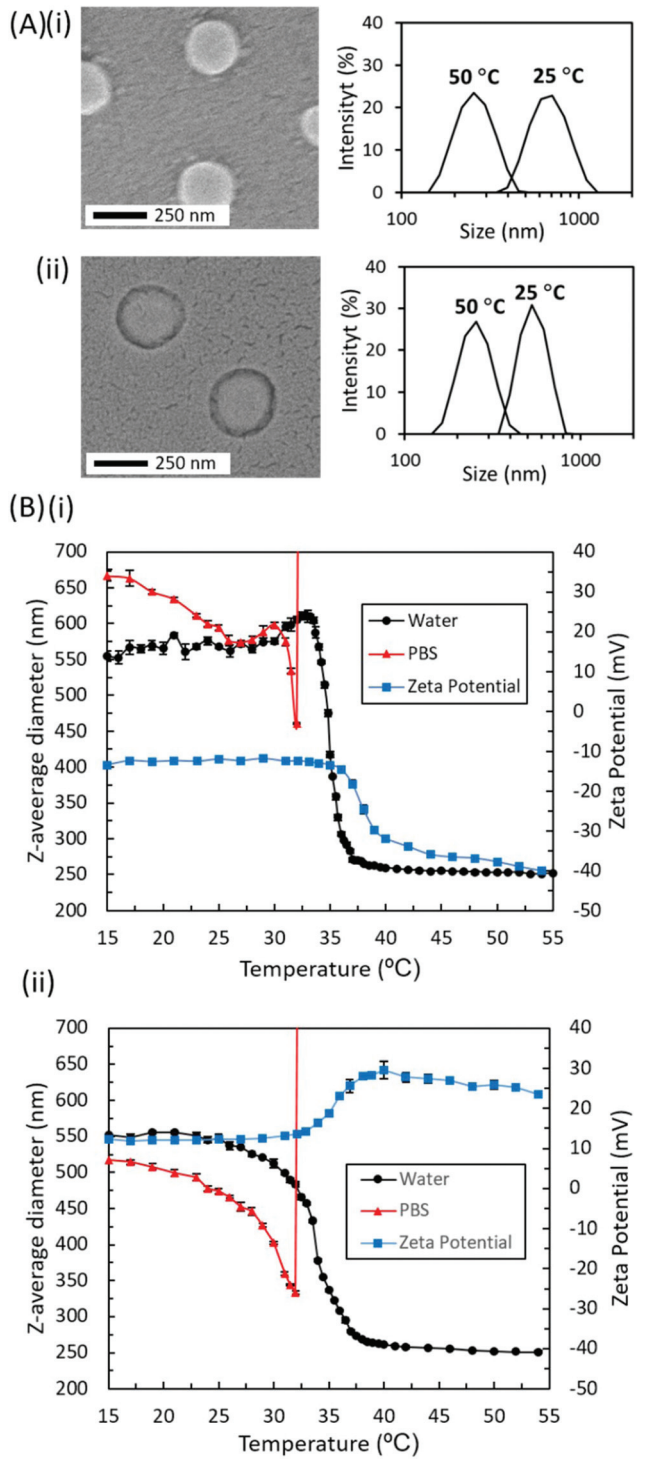

Fig. 2 Characterisation of PNA-00 and PNA-25 microgels by dynamic light scattering, laser Doppler electrophoresis and SEM. (A) SEM images of the dried microgel particles and DLS size distribution by intensity at 25 °C (i) PNA-00 (ii) PNA-25. (B) Temperature dependence of the hydrodynamic diameter in either water or phosphate buffered saline (PBS) and zeta potential of (i) PNA-00 (ii) PNA-025 in water.

Z-average diameter at the VPTT, Fig. 2(B)(i), as first shown by Pelton *et al.*[58] In the presence of salts at physiological concentrations (0.137 M) the particles flocculate as they reach the VPTT, indicated by the dramatic increase in *Z*-average diameter beyond 32 °C.[39] The sample containing 25 mol% AlA (PNA-25) showed the same colloidal stability in water and triggered flocculation in PBS, Fig. 2(B)(ii). The salt-responsive flocculation of the microgels was also investigated with a range of NaCl concentrations. Increasing the NaCl concentration resulted in the aggregation temperature decreasing due to the poorer solvent environment for the PNIPAM. PNA-00 and PNA-25 were both found to show similar responses, Table 3. Previous work by Vincent *et al.* has shown that PNIPAM microgels synthesised with BIS and a sulphate initiator flocculate in NaCl above a concentration of 0.025 M when raising the temperature.[43] At a low NaCl concentration the interparticle electrostatic repulsion was great enough to prevent flocculation. At higher concentrations these electrostatic forces are weakened enough to allow flocculation. Analysis of the zeta potential of PNA-00 with increasing temperature in water displayed an initial negative zeta-potential of −12 mV up to 25 °C, attributed to the KPS providing a negative surface charge on the microgels through its incorporation at the polymer chain ends. As the temperature increases above the VPTT the zeta potential shows a corresponding decrease to >−40 mV as the surface charge density increases with the decrease in particle surface area, and the chains ends collapse onto the surface. For sample PNA-25 the zeta potential was positive, indicating successful incorporation of a proportion of the AlA comonomer to give a cationic charge that counters the anionic charge of the chain ends. When the particles were heated above their VPTT the zeta potential increased as the reduction in size resulted in an increase in charge density. The two microgels show temperature and salt responsive behaviour, with flocculation only occurring when both the temperature is above the VPTT and the ionic strength is sufficient. This is ideal for triggered aggregation in response to physiological conditions in an ISFI system.

3.2 PNIPAm microgel aggregate studies

Given the propensity for the microgels to flocculate in a dilute dispersion, the concentration of the dispersion was increased to determine whether bulk aggregation on a macroscopic scale was possible. The relative hydrophilicity of each microgel was measured by its % (w/w) water content above and below the VPTT. The concentration (% (w/w)) of PNA-00 and PNA-25 in

Table 3 Microgel flocculation in NaCl

	Aggregation temperature[a] (°C)	
[NaCl] (mol L^{-1})	PNA-00	PNA-25
0.001	—	—
0.010	—	—
0.100	34	42
1.000	24	24

[a] Samples heated in 1 °C intervals from 15 to 55 °C. Flocculation indicated by large increase in *Z*-Ave, as shown in Fig. 2.

PBS at 25 °C was increased and studied *via* the tube inversion method until a gel was formed. The concentration required for a self-supporting gel was 6.24% (w/w) for PNA-25 and 14.90% (w/w) for PNA-00. Previous work has shown that PNIPAm microgels which are polyampholytic in nature swell as the ionic strength of the solvent increases,[59] hence a lower (% w/w) of PNA-25 is required to form a self-supporting gel. Upon heating to 37 °C both gels aggregate and expel solvent in the process. The microgels formed a phase separated disc shape of aggregated material, due to the cylindrical shape of the vial used, Fig. 3. The formation of aggregate over time can also be seen in ESI Fig. S4,† showing that the time for both samples to form dense aggregates was approximately 90 minutes. The aggregated form of the microgels was seen as the surface charge of the microgel was not great enough to form a shrunken gel.[60] This process was reversible, after being held at 37 °C for 1 hour and cooling, the aggregate returned to a self-supporting gel that re-adsorbed the expelled solvent within 1 hour. The water content of PNA-00 and PNA-25 were measured both above and below the VPTT. Below the VPTT the water content of the samples were 85.1% and 93.8% for PNA-00 and PNA-25 respectively. The hydrophilic nature of AlA is independent of temperature,[61] hence the sample containing AlA, PNA-25, remained much more hydrophilic above the VPTT (at 37 °C) containing 76.8% w/w water while PNA-00 contained only 34.5% water. This difference in the water content of the aggregates was reflected in the reduction in volume when the swollen gel forms an aggregate. The swollen gel of PNA-00 had a larger percentage reduction in volume than PNA-25 upon forming an aggregate. This data is summarised in Table 4. Despite the PNA-00 swollen gel being formed of 14.90% (w/w) microgel, its % reduction in volume upon aggregation was greater than the lower microgel content of 6.24% (w/w) in the PNA-25 swollen gel. This suggests the aggregate of PNA-25 contained a greater volume of free space between aggregated microgel particles, owing to its smaller % volume reduction upon aggregate formation. The structure of the aggregates was investigated further *via* SEM and AFM imaging. Samples of the PNA-00 and PNA-25 aggregates were dried and imaged by SEM (shown in Fig. 4A and B respectively). The

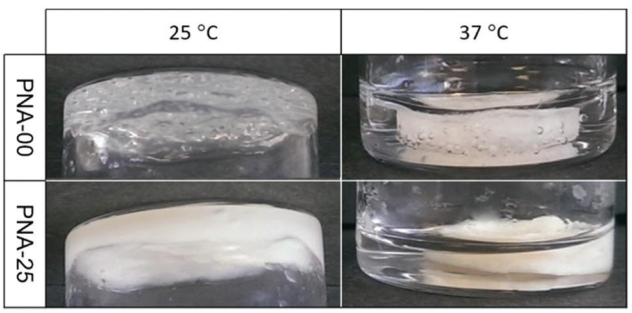

Fig. 3 Images of dual-responsive transition of the microgels in PBS; from swollen self-supporting gels to bulk aggregates. Microgel samples as swollen gel (left) and bulk aggregate (right). PNA-00 (top) and PNA-25 (bottom).

Table 4 Water content of the microgels at 25 °C and 37 °C and change in volume

Sample	% (w/w) of water contained within the sample		% reduction in volume upon forming aggregate[a]
	25 °C	37 °C	
PNS-00	85.1	34.5	76
PNA-25	93.8	76.8	66

[a] The height and diameter of the cylindrical swollen gel and corresponding aggregate were used to calculate the change in volume (see ESI Fig. 4 for images of the samples).

PNA-25 aggregate displayed a dense structure with a tendency to film-form while the PNA-25 aggregate presented a looser structure in which individual particles could easily be distinguished. AFM analysis was then utilised to assess the topography of the samples, (Fig. 4C and D for PNA-00 and PNA-25 respectively) these images revealed that PNA-25 presented a fibrous structure compared to the irregular structure of PNA-00. The differences in the topography of the samples are clearly shown in the 3D representation of the AFM characterisation, Fig. 4E for PNA-00 and Fig. 4F for PNA-25. The surface of the PNA-25 aggregate was much rougher (roughness (R_q) value of 267 nm) compared to PNA-00 (R_q value of 182 nm) and PNA-25 revealed potential pores between the fibres. This fibrous structure of the PNA-25 aggregates was not expected and is an aspect for further investigation in the future. The difference between the two aggregates explains the higher water content of PNA-25 due to its greater porosity and may alter the rate of drug release from the aggregates.

The propensity for the microgels to flocculate in response to both temperature and salt could be utilised to give a macroscopic aggregate at high microgel concentrations. Potentially the relative hydrophilicity and porosity of the aggregates can be tuned by mixing PNA-00 and PNA-25 due to their different water content and apparent structural differences in aggregated form.

Upon injection as an ISFI the swollen gel will be in contact with interstitial fluid, which contains the metal ions magnesium and calcium as part of a complex mixture of inorganic salts.[62] This inorganic salt composition was simulated by Hank's balanced salt solution (HBSS). Therefore, in order to more closely mimic the ionic environment *in vivo* the aggregation of the microgels was assessed in HBSS instead of PBS. Aggregation was found to occur in HBSS (see ESI Fig. S5†) in a similar manner to the PBS studies and hence the different metal ions present in HBSS were not found to inhibit the aggregation process.

3.3 Injection of microgels into tissue mimic

Given that formation of the depot aggregate occurs upon exposing the concentrated microgels to physiological conditions we next assessed the suitability of injection into tissue. For this purpose we utilised agarose gel as a subcutaneous

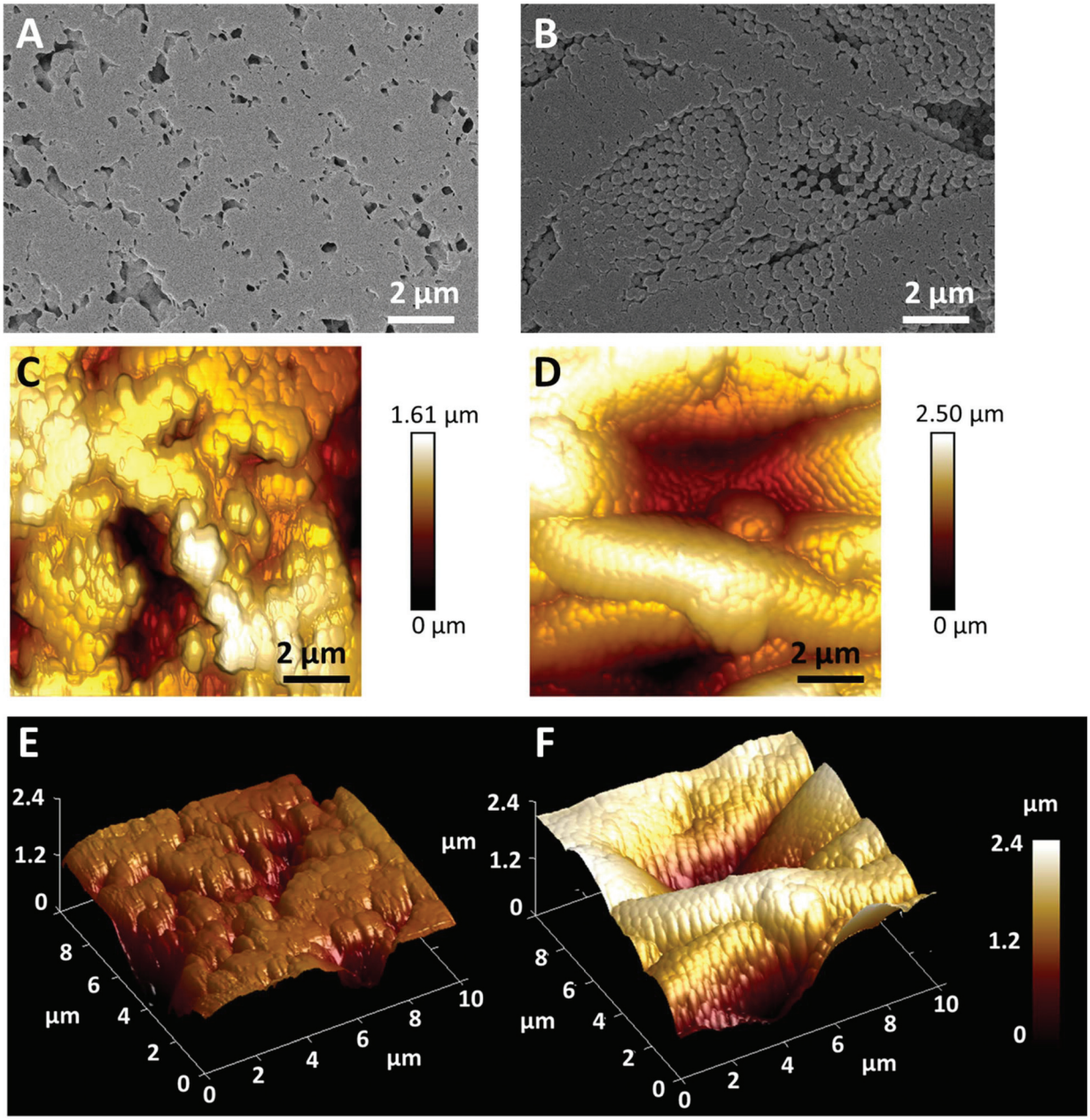

Fig. 4 Characterisation of microgel aggregates. (A, B) SEM images, (C, D) AFM images and (E, F) 3D representations of (C, D) respectively. PNA-00 shown in (A, C, E) and PNA-25 in (B, D, F).

tissue mimic[63] at 37 °C. The concentrated microgel at ambient temperature was injected into the tissue mimic through a hypodermic needle. The sheer thinning properties of PNIPAm microgels allowed the swollen gel of PNA-00 and PNA-25 to be injected through a 18G needle. This is followed by rapid aggregation of the particles into a depot. Additionally, depot formation was also possible with a much lower microgel concentration; PNA-25 was injected as a liquid at 2.0% (w/w) and displayed the same aggregation behaviour as higher microgel concentrations, Fig. 5 (see video in ESI†). The ability to obtain depot formation at lower concentrations is beneficial as a liquid is more desirable for ease of formulation with drug and loading into a syringe for as an ISFI.[17] The microgel aggregate formed a planar depot that is most likely due to the fracturing of the agarose gel by the hypodermic needle, and the subsequent filling of the void by the microgel outwards along the fault line.

3.4 Polystyrene nanoparticle entrapment study

An ISFI will ideally display no initial burst release, therefore in our system as the microgels aggregate they should be able to rapidly entrap a payload of drug containing nanoparticles with high entrapment efficiency.[24] To probe this ability, oil red O dye-containing polystyrene (PS) nanoparticles were synthesised

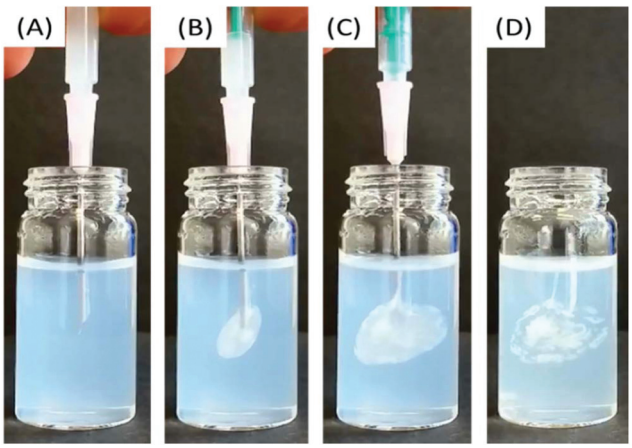

Fig. 5 Image showing injection of PNA-25 through 18G hypodermic needle into 37 °C agarose gel, followed by aggregation of material at time points (A) 0 (B) 5 (C) 12 and (D) 19 seconds.

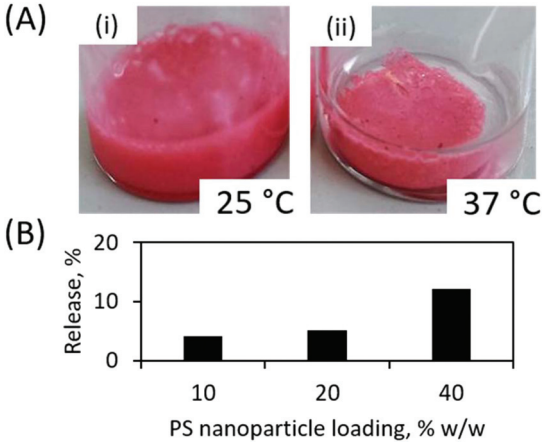

Fig. 6 (A) (i) Swollen gel composite of 40% (w/w) PS nanoparticle loaded into PNA-25 at 25 °C and (ii) aggregation of composite at 37 °C with entrapment of PS nanoparticles. (B) Percentage of total PS particles released 1 hour after aggregation of composite.

as a model payload which mimics the entrapment of solid drug nanoparticles. Like solid drug nanoparticles, oil red O dye-containing PS nanoparticles can form a nanosuspension in water, and are a similar size, however the oil red O within the PS particles allows quantification of the amount released using UV-Vis spectroscopy. Firstly, the PS particles were synthesised using adaptations from a previously published dispersion polymerisation method.[47] The PS nanoparticles were then dyed with the hydrophobic dye Oil Red O (OR),[48] so that the release could be quantified at a wavelength of 580 nm where there is negligible absorbance by any potential PNIPAm fragments lost from the aggregate. These dye containing particles will be denoted as PS-OR. The PS colloids were characterised using DLS after synthesis and when dispersed into PBS as PS-OR after dying and lyophilisation (see Table 5). The slightly larger *Z*-average diameter after dying can be accounted for by entrapment of dye. SEM images revealed that monodisperse particles with spherical morphology were synthesised, (see ESI, Fig. S6†). Nanocomposites containing PS-OR nanoparticles were then prepared. Firstly, PNA-25 was dispersed at 6.24% (w/w) in PBS to give a swollen gel and then PS-OR nanoparticles were mixed into the gel at 10, 20 and 40% (w/w) *vs*. PNA-25. These samples remained as swollen self-supporting gels even with 40% (w/w) PS-OR nanoparticles loaded, Fig. 6(A)(i).

Upon heating to 37 °C to induce aggregation, the expelled solvent is visibly colourless, suggesting that PS-OR particles remained entrapped as a nanocomposite with the microgel Fig. 6(A)(ii). This burst release behaviour was quantified by UV-Vis to determine the concentration of PS-OR particles in the expelled liquid (see ESI, Fig. S7†). This analysis showed low burst release (<13%) for all samples but that increasing the concentration of PS-OR nanoparticles led to greater burst release, Fig. 6(B). This data indicates the microgels are able to retain the majority of a nanoscale payload distributed through the nanocomposite as it aggregates from a swollen gel. This is despite a substantial volume of PBS being expelled from the polymer network of the contracting microgel particles.

Table 5 PS nanoparticle properties

PS after synthesis		PS-OR dispersed in PBS	
Z-Average diameter (nm)	PdI	*Z*-Average diameter (nm)	PdI
802 ± 14	0.05 ± 0.03	821 ± 25	0.05 ± 0.04

3.5 *In vitro* release study

To test the release rate of drug from the microgel aggregates *in vitro*, formulations were created from the mixing of poorly water-soluble antiretroviral drug lopinavir (LPV) in its powder form, or solid drug nanoparticle (SDN) form, into swollen gels (the different formulations are shown in Table 6). LPV is a potent HIV-specific protease inhibitor which is administered in combination with ritonavir as a booster and requires daily oral dosing for life.[64,65] We selected LPV as the model hydrophobic drug in our study given its very low aqueous solubility

Table 6 Formulations of microgel-drug for ISFI's

Formulation	LPV (mg)	LPV SDN[a] (mg)	PNA-00 (mg)	PNA-25 (mg)	% (w/w) water[b]
Free SDN	—	44.4	—	—	—
PNA-25-SDN	—	44.4	—	66.6	76.8
PNA-00/25-SDN	—	44.4	87.5	33.3	56.4[c]
PNA-00-SDN	—	44.4	175	—	34.5
PNA-25-LPV	22.2	—	—	66.6	76.8

[a] LPV SDNs consist of 50% (w/w) LPV the remainder is 40% PVA and 10% Kolliphor TPGS. [b] % (w/w) of water in aggregate at 37 °C. [c] Calculated from: ∑ amount of water contained in mass of each microgel, and total mass of microgel in formulation.

(predicted to be 0.00192 mg mL^{-1}) and on-going evaluation of LPV SDNs in clinical trial (clinicaltrials.gov reference NCT02631473). The LPV SDNs had a *Z*-average diameter of 330 nm and PdI of 0.18 (see ESI Fig. S8†). Swollen gels were used so that aggregated disk shaped samples formed upon heating, to simplify sampling release media in the release experiment (see ESI Fig. S9†). Utilising the large difference in the water content and porosity of the PNA-00 and PNA-25 aggregated microgel materials at 37 °C, Table 4, allows the two microgel samples to be mixed in different ratios to tune the water content of the aggregate. Poorly water soluble drugs have been shown to have a slower release rate from an insoluble matrix than more water soluble drug,[66] hence we expected the water content and structure of the aggregates to control the rate of release of drug. PNA-00 and PNA-25 were used with a mass of each that gave a self-supporting gel at room temperature in 1 mL of PBS, and 56.4% (w/w) water in the aggregated form (denoted as PNA-00/25-SDN), giving an intermediate water content between that of the two microgels when used separately. The release of drug into the PBS surrounding the microgel/SDN nanocomposites was then measured over time using HPLC. Due to the low saturation concentration of the drug, the release media was completely removed and replaced during the release experiment.[10] The nanocomposite showed excellent mechanical stability, remaining in its original shape over the complete release period. Comparing the release of LPV from the formulations PNA-25-SDN, PNA-00/25-SDN and PNA-00-SDN it can be seen that if the depot has a higher % (w/w) water content the release rate is enhanced, leading to a larger total cumulative release after 120 days, Fig. 7. This effectively allows us to tune the release rate from the depot. Based on the characterisation of the aggregate with SEM and AFM we speculate that this could be due to the formation of a more porous structure containing more water, which has been linked with faster drug release.[46] Solute transport from non-degradable polymeric systems is mainly considered as diffusion driven, with matrix-type devices showing Fickian diffusion.[67] We applied the Higuchi model of drug release,[68] which describes drug release from a matrix system to our release data.[69] We used the simplified Higuchi model, see Fig. 7(c).[70,71] This suggests that for PNA-25-SDN and PNA-00/25-SDN there are two phases or release (**I** and **II**). In phase **I** the porosity introduced by PNA-25 could allow SDNs to be released from the aggregate, giving a much larger dissolution constant than the other formulations, Table 7. This is followed by phase **II** where it appears that the remainder of the SDNs are unable to diffuse out of the aggregate and instead are released as drug molecules which then diffuse with a dissolution constant similar to the other formulations. PNA-00-SDN and PNA-25-LPV only displayed one release phase. PNA-00-SDN only contains PNA-00 microgel which forms a much less porous structure, suggesting there is only release of drug molecules rather than SDN's. In PNA-25-LPV the lopinavir drug was in the form of a micron-sized powder (see ESI Fig. S10†), not as SDNs. Hence no two stage release is seen, as the large powder particles are not able to diffuse through the aggregate and instead only dissolved drug molecules are released.

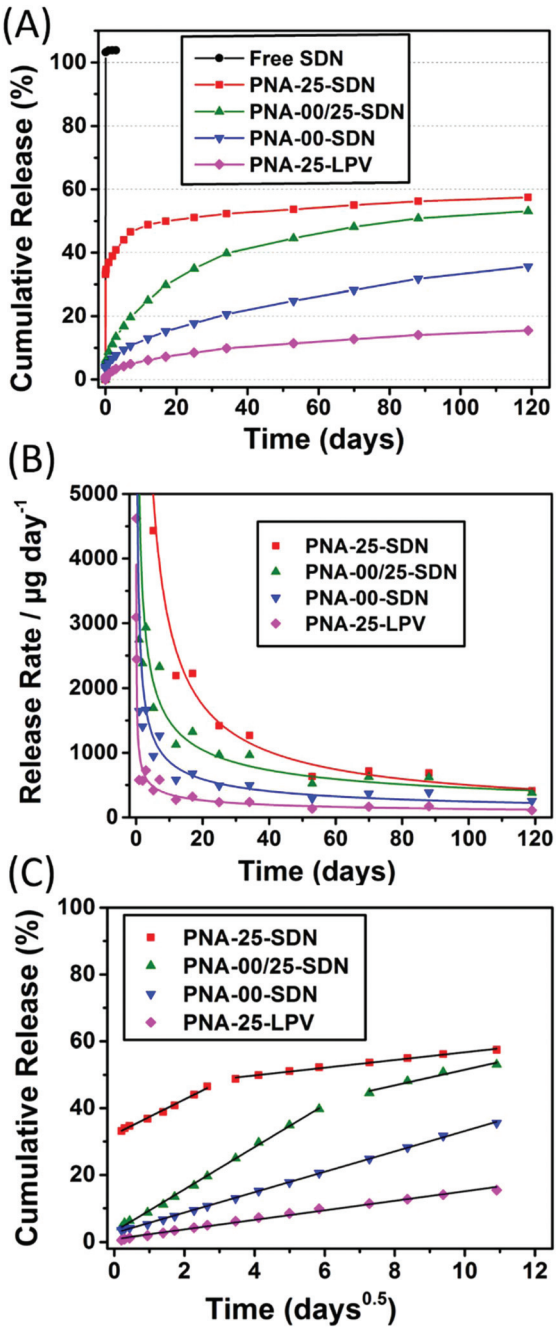

Fig. 7 Release of LPV drug from aggregated microgel discs over 120 days; quantified by HPLC analysis. An SDN control without microgel, 'Free SDN', was performed. After 120 days the depot was dissolved in acetonitrile for HPLC analysis to check remaining drug + amount released = 100% (A) cumulative release (B) release rate, lines are guides for the eye (C) application of the Higuchi model to the LPV release over 120 days.

The burst release from the initial aggregation of the disk is only 4.3% and 3.4% for PNA-00/25-SDN and PNA-00-SDN respectively. The PNA-25-SDN nanocomposite was the only

Table 7 Correlation coefficient (R_c) and Higuchi dissolution constant (k_H)

	Phase I		Phase II	
Formulation	R_c	k_H days$^{-0.5}$	R_c	k_H days$^{-0.5}$
PNA-25	0.994	5.25	0.993	1.16
PNA-00/25-SDN	0.999	6.33	0.966	2.34
PNA-00-SDN	0.999	3.05	—	—
PNA-25-LPV	0.992	1.43	—	—

sample to show appreciable burst release of 33.1%. As seen in the SEM/AFM analysis in Fig. 4 the PNA-25 microgel aggregate was the most porous, therefore it is possible that the SDNs near the surface of the aggregate were squeezed out rapidly through the pores during the initial aggregation, leading to a burst release. This theory is also supported by the concentration of LPV obtained during the burst release, much higher than the solubility of the hydrophobic drug lopinavir which would only be possible if the drug was released in SDN form. However, the water content of PNA-00/25-SDN nanocomposite was also reasonably high at 56.4% (w/w) and may have presented porosity and yet very little burst release was found. This difference could also be attributed to different particle packing; the opposite surface charges in PNA-00/25-SDN may lead to attractive interactions between microgel particles reducing the porosity of the material. This behaviour will be further studied in our future work. The formulation PNA-25-LPV, which contains the drug in powdered form, rather than as an SDN, displayed the slowest release rate with total release lower than all the SDN formulations, despite being loaded into the most porous depot formed from PNA-25. Hence, loading drug in SDN form allows the release rate from the depot to be enhanced, likely due to the much greater surface area of the SDNs assisting dissolution;[72] or their amorphous nature,[49] which aids in dissolution rate of drugs *vs.* crystalline drug form.[73] This behaviour potentially offers an additional mechanism of controlling the rate of drug release from the nanocomposite. In powdered drug form the burst release is also minimal at 0.5%, despite the SDNs having a 33.1% burst release from the same PNA-25 microgel. This reinforces the idea of porosity being linked to water content of the aggregates, with small nanoparticulates releasing at a greater rate than the powdered form of the drug.

Although the release rate was not clinically relevant for LPV we have demonstrated sustained release and the potential for the rate of release to be tuneable for the drug and it's SDN form. Hence, this system should be applicable to other more clinically relevant poorly water-soluble drugs. These release studies showed that the rate of release of dissolved drug molecules can be tuned by blending microgels with different polymer composition, and by varying the form of the drug.

3.6 Cytotoxicity study

PNIPAm has been widely used as a potential material for drug delivery and has been shown not to display cytotoxic properties

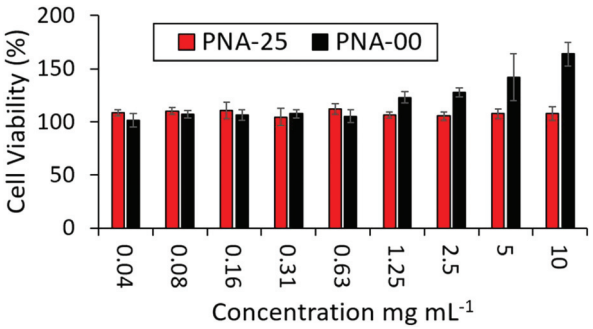

Fig. 8 Cytotoxicity of microgels towards cells in ATP assay.

in numerous studies including PNIPAm in microgel form.[74–76] Additionally, Kjøniksen *et al.* have revealed that even at a high concentration PNIPAm microgels are not cytotoxic.[46]

The ATP, Fig. 8, and MTT (see ESI Fig. S11†) assays showed that when MDCK-II cells were incubated with PNA-00 and PNA-25 for 72 hours, at concentrations ranging from 0.04 mg ml^{-1} to 10 mg ml^{-1}, no sign of cell toxicity could be detected. The positive control rotenone was characterised by reduced cell viability compared to the control at all tested concentrations (from 0.19 μM to 100 μM). It can be concluded that the MTT assay could correctly detect reduction of mitochondrial activity in the presence of PNA-00 and PNA-25 and lack of direct effect on this cell function in the presence of rotenone. The ATP assay could measure the cell viability by measuring the luminescent signal given out when beetle luciferin is oxidised to oxyluciferin in the presence of ATP obtained from the cells after lysis. Considering the nature of the MTT and ATP assay, other cytotoxic effects cannot be dismissed; consequently, future investigations to support the development of PNA-00 and PNA-25 clinical applications should include a comprehensive evaluation of cellular, immunological and tissue toxicities.

4. Conclusion

PNIPAm and PNIPAm-*co*-AlA microgels were found to provide a long term sustained release of the hydrophobic drug LPV and its SDN form. PNIPAm microgels could be formulated to contain a nanoparticulate payload to form an injectable nanocomposite material in response to a dual stimulus of temperature and salt. The system overcomes some of the common problems associated with ISFIs that have previously been developed. For example, the formulation with drug was simple to perform, it was easily injectable through a minimally invasive hypodermic needle, showed minimal burst release, and mechanical stability throughout the release. Sustained release of drug from the material was also maintained for a period of at least 120 days. The potential to easily tune the release rate from the system by adjusting the ratio of the two microgel species PNA-00 and PNA-25, or enhance the release rate of the drug by using the form of SDNs was also demonstrated. This

drug delivery system should be applicable to other hydrophobic drugs, and cytotoxicity is not an issue.

This makes the system a suitable candidate as an ISFI for hydrophobic drugs and SDNs, where injections could possibly be given as infrequently as twice a year to improve adherence rates in the treatment of long term and particularly chronic conditions. The inflammation response at the depot site still requires investigation. There is also the potential to release multiple drugs as a combination therapy.

Acknowledgements

We gratefully acknowledge financial support from the EPSRC (Grant Number EP/M01973X/1) and a DTA studentship, and the Royal Society (RG140213). The authors would also like to thank the Centre for Materials Discovery and Prof. Steve Rannard for access to equipment and technical support. We are grateful to Zhuola (School of Engineering) for assistance with the AFM imaging. Additionally, we thank Prof. Peter Myers and Richard Hayes for HPLC technical support.

References

1 E. Sabaté, *Adherence to Long-Term Therapies: Evidence for Action*, World Health Organisation, Geneva, Switzerland, 2003.
2 M. R. DiMatteo, *Med. Care*, 2004, **42**, 200–209.
3 A. J. Claxton, J. Cramer and C. Pierce, *Clin. Ther.*, 2001, **23**, 1296–1310.
4 B. Winner, J. F. Peipert, Q. Zhao, C. Buckel, T. Madden, J. E. Allsworth and G. M. Secura, *N. Engl. J. Med.*, 2012, **366**, 1998–2007.
5 G. Rossi, S. Frediani, R. Rossi and A. Rossi, *BMC Psychiatry*, 2012, **12**, 122.
6 S. Rietveld and J. M. Koomen, *Dis Manage. Health Outcomes*, 2002, **10**, 621–630.
7 C. M. Negrín, A. Delgado, M. Llabrés and C. Évora, *Biomaterials*, 2001, **22**, 563–570.
8 A. L. Kjøniksen, M. T. Calejo, K. Zhu, A. M. S. Cardoso, M. C. P. De Lima, A. S. Jurado, B. Nyström and S. A. Sande, *J. Pharm. Sci.*, 2014, **103**, 227–234.
9 J. F. Remenar, *Mol. Pharm.*, 2014, **11**, 1739–1749.
10 J. C. Wright and D. J. Burgess, *Long Acting Injections and Implants*, Springer-Verlag, Berlin, 2012.
11 S. Freiberg and X. X. Zhu, *Int. J. Pharm.*, 2004, **282**, 1–18.
12 A. S. Hoffman, *J. Controlled Release*, 2008, **132**, 153–163.
13 R. K. Subedi, S. Y. Oh, M.-K. Chun and H.-K. Choi, *Arch. Pharm. Res.*, 2010, **33**, 339–351.
14 C. B. Packhaeuser, J. Schnieders, C. G. Oster and T. Kissel, *Eur. J. Pharm. Biopharm.*, 2004, **58**, 445–455.
15 A. Chenite, C. Chaput, D. Wang, C. Combes, M. Buschmann, C. Hoemann, J. Leroux, B. Atkinson, F. Binette and A. Selmani, *Biomaterials*, 2000, **21**, 2155–2161.
16 D. Y. Ko, U. P. Shinde, B. Yeon and B. Jeong, *Prog. Polym. Sci.*, 2013, **38**, 672–701.
17 E. Ruel-Gariépy and J. C. Leroux, *Eur. J. Pharm. Biopharm.*, 2004, **58**, 409–426.
18 A. Hatefi and B. Amsden, *J. Controlled Release*, 2002, **80**, 9–28.
19 A. Fakhari and J. Anand Subramony, *J. Controlled Release*, 2015, **220**, 465–475.
20 H. Kranz and R. Bodmeier, *Int. J. Pharm.*, 2007, **332**, 107–114.
21 B. Jeong and A. Gutowska, *Trends Biotechnol.*, 2002, **20**, 305–311.
22 L. Pescosolido, PhD Thesis, Sapienza University of Rome, 2011.
23 B. Jeong, Y. H. Bae, D. S. Lee and S. W. Kim, *Nature*, 1997, **388**, 860–862.
24 S. Kempe and K. Mäder, *J. Controlled Release*, 2012, **161**, 668–679.
25 S. Sareen, L. Joseph and G. Mathew, *Int. J. Pharm. Invest.*, 2012, **2**, 12.
26 B. E. Rabinow, *Nat. Rev. Drug Discovery*, 2004, **3**, 785–796.
27 S. Ranjita, *J. Pharm. Invest.*, 2013, **43**, 1–26.
28 T. O. Mcdonald, M. Siccardi, D. Moss, N. Liptrott, M. Giardiello, A. Owen and S. Rannard, *in The application of nanotechnology to drug delivery in Medicine*, Elsevier Health Sciences, Toronto, 2014, pp. 1–500.
29 T. O. McDonald, L. M. Tatham, F. Y. Southworth, M. Giardiello, P. Martin, N. J. Liptrott, A. Owen and S. P. Rannard, *J. Mater. Chem. B*, 2013, **1**, 4455–4465.
30 T. O. McDonald, P. Martin, J. P. Patterson, D. Smith, M. Giardiello, M. Marcello, V. See, R. K. O'Reilly, A. Owen and S. Rannard, *Adv. Funct. Mater.*, 2012, **22**, 2469–2478.
31 T. O. McDonald, M. Giardiello, P. Martin, M. Siccardi, N. J. Liptrott, D. Smith, P. Roberts, P. Curley, A. Schipani, S. H. Khoo, J. Long, A. J. Foster, S. P. Rannard and A. Owen, *Adv. Healthcare Mater.*, 2014, **3**, 400–411.
32 M. Boffito, A. Jackson, A. Owen and S. Becker, *Drugs*, 2014, **74**, 7–13.
33 R. H. Pelton and P. Chibante, *Colloids Surf.*, 1986, **20**, 247–256.
34 B. R. Saunders and V. B, *Adv. Colloid Interface Sci.*, 1999, **80**, 1–25.
35 M. Das, H. Zhang and E. Kumacheva, *Annu. Rev. Mater. Res.*, 2006, **36**, 117–142.
36 S. Chen, J. Long and Y. Dan, *J. Appl. Polym. Sci.*, 2011, **121**, 3322–3331.
37 B. R. Saunders, N. Laajam, E. Daly, S. Teow, X. Hu and R. Stepto, *Adv. Colloid Interface Sci.*, 2009, **147–148**, 251–262.
38 K. Kratz, T. Hellweg and W. Eimer, *Colloids Sur., A*, 2000, **170**, 137–149.
39 R. Pelton, *Adv. Colloid Interface Sci.*, 2000, **85**, 1–33.
40 M. Muratalin and P. F. Luckham, *J. Colloid Interface Sci.*, 2013, **396**, 1–8.
41 W. McPhee, K. C. Tam and R. Pelton, *J. Colloid Interface Sci.*, 1993, **156**, 24–30.

42 N. Al-manasir, S. Fanaian, K. Zhu, B. Nyström, G. Karlsson and A. Kjøniksen, *J. Phys. Chem. B*, 2009, **113**, 11115–11123.
43 M. Rasmusson, A. Routh and B. Vincent, *Langmuir*, 2004, **20**, 3536–3542.
44 R. Mohsen, G. J. Vine, N. Majcen, B. D. Alexander and M. J. Snowden, *Colloids Surf., A*, 2013, **428**, 53–59.
45 M. J. Snowden, J. C. Morgan and B. Vincent, *UK Patent*, GB2262117A, 1993.
46 A. L. Kjøniksen, M. T. Calejo, K. Zhu, A. M. S. Cardoso, M. C. P. De Lima, A. S. Jurado, B. Nyström and S. A. Sande, *J. Pharm. Sci.*, 2014, **103**, 227–234.
47 H. Zhang, J. Y. Lee, A. Ahmed, I. Hussain and A. I. Cooper, *Angew. Chem.*, 2008, **47**, 4573–4576.
48 J. H. Lee, I. J. Gomez, V. B. Sitterle and J. C. Meredith, *J. Colloid Interface Sci.*, 2011, **363**, 137–144.
49 M. Giardiello, N. J. Liptrott, T. O. Mcdonald, D. Moss, M. Siccardi, P. Martin, D. Smith, R. Gurjar, S. P. Rannard and A. Owen, *Nat. Commun.*, 2016, **7**, 13184.
50 J. Shen and D. J. Burgess, *J. Pharm. Pharmacol.*, 2012, **64**, 986–996.
51 H. Hyun, Y. H. Kim, I. B. Song, J. W. Lee, M. S. Kim, G. Khang, K. Park and H. B. Lee, *Biomacromolecules*, 2007, **8**, 1093–1100.
52 A. D'Avolio, L. Baietto, M. Siccardi, M. Sciandra, M. Simiele, V. Oddone, S. Bonora and G. Di Perri, *Ther. Drug Monit.*, 2008, **30**, 662–669.
53 C. Hoskins, P. K. T. Lin, L. Tetley and W. P. Cheng, *Polym. Adv. Technol.*, 2012, **23**, 710–719.
54 S. Chen, X. Jiang and L. Sun, *J. Appl. Polym. Sci.*, 2013, **130**, 1164–1171.
55 X. Ma, Y. Cui, X. Zhao, S. Zheng and X. Tang, *J. Colloid Interface Sci.*, 2004, **276**, 53–59.
56 K. Ogawa, A. Nakayama and E. Kokufuta, *Langmuir*, 2003, **19**, 3178–3184.
57 S. Ito, K. Ogawa, H. Suzuki, B. Wang, R. Yoshida and E. Kokufuta, *Langmuir*, 1999, **15**, 4289–4294.
58 R. H. Pelton, H. M. Pelton, A. Morphesis and R. L. Rowell, *Langmuir*, 1989, **5**, 816–818.
59 M. Das and E. Kumacheva, *Colloid Polym. Sci.*, 2006, **284**, 1073–1084.
60 J. Zhou, G. Wang, L. Zou, L. Tang, M. Marquez and Z. Hu, *Biomacromolecules*, 2008, **9**, 142–148.
61 G. Huang, J. Gao, Z. Hu, J. V. St John, B. C. Ponder and D. Moro, *J. Controlled Release*, 2004, **94**, 303–311.
62 N. Fogh-Andersen, B. M. Altura, B. T. Altura and O. Siggaard-Andersen, *Clin. Chem.*, 1995, **41**, 1522–1525.
63 F. Ye, S. W. Larsen, A. Yaghmur, H. Jensen, C. Larsen and J. Østergaard, *Eur. J. Pharm. Sci.*, 2012, **46**, 72–78.
64 H. L. Sham, D. J. Kempf, A. Molla, K. C. Marsh, G. N. Kumar, C. M. Chen, W. Kati, K. Stewart, R. Lal, A. Hsu, D. Betebenner, M. Korneyeva, S. Vasavanonda, E. McDonald, A. Saldivar, N. Wideburg, X. Chen, P. Niu, C. Park, V. Jayanti, B. Grabowski, G. R. Granneman, E. Sun, A. J. Japour, J. M. Leonard, J. J. Plattner and D. W. Norbeck, *Antimicrob. Agents Chemother.*, 1998, **42**, 3218–3224.
65 V. Oldfield and G. L. Plosker, *Drugs*, 2006, **66**, 1275–1299.
66 S. Allababidi and J. C. Shah, *J. Pharm. Sci.*, 1998, **87**, 738–744.
67 Y. Fu and W. J. Kao, *Pharm. Res.*, 2009, **7**, 429–444.
68 T. Higuchi, *J. Pharm. Sci.*, 1961, **50**, 874–875.
69 F. Ganji and E. Vasheghani-Farahani, *Iran. Polym. J.*, 2009, **18**, 63–88.
70 D. Samaha, R. Shehayeb and S. Kyriacos, *Dissolution Technol.*, 2009, **16**, 41–46.
71 T. Higuchi, *J. Pharm. Sci.*, 1963, **52**, 1145–1149.
72 E. Merisko-Liversidge and G. G. Liversidge, *Adv. Drug Delivery Rev.*, 2011, **63**, 427–440.
73 M. P. B. C. Hancock, *Pharm. Res.*, 2000, **17**, 397–404.
74 P. C. Naha, K. Bhattacharya, T. Tenuta, K. A. Dawson, I. Lynch, A. Gracia, F. M. Lyng and H. J. Byrne, *Toxicol. Lett.*, 2010, **198**, 134–143.
75 M. A. Cooperstein and H. E. Canavan, *Biointerphases*, 2013, **8**, 19.
76 W. Xiong, X. Gao, Y. Zhao, H. Xu and X. Yang, *Colloids Surf., B*, 2011, **84**, 103–110.